PAPER

Check for updates

Mechanically robust but dynamic elastomers as functional coatings based on dynamic covalent bonds and multiple noncovalent interactions†

Xiao Yang,[a] Dianteng Zhao,[a] Yichen Huang,[a] Xinyun Li,*[b] Bo Zheng [ID] *[a] and Lingyan Gao [ID] *[a]

Much attention has been paid to the fabrication of advanced materials to solve the global plastic pollution crisis. This study developed a sustainable coating material, **Poly(TA-DES-Cu)**, a thioctic acid-based covalent adaptable network (CAN). The synergistic noncovalent interactions of Cu^{2+}–carboxyl coordination and DES-involved hydrogen bonding in **Poly(TA-DES-Cu)** endow the elastomer with good mechanical properties (1808% fracture strain and 7.92 MJ m^{-3} toughness), self-healing capability (25–60 °C, >80% stress recovery after 10 cycles), interfacial adhesion (2.52 MPa on steel) and recyclability. In particular, the cooperative dynamic noncovalent interactions and molecular chain slippage enable efficient energy dissipation and puncture resistance (11.42 mJ), leading to its further application as a coating material. After coating on nonwoven fabrics, it not only enhances the mechanical performance but also leads to broad-spectrum antibacterial activity of the resulting composite material. This strategy provides a novel approach for designing sustainable intelligent polymer materials.

Introduction

Developing recyclable polymers and designing effective (bio) degradable materials represent pivotal challenges in combating the global plastic pollution crisis.[1–3] Recently, covalent adaptable networks (CANs) linked by dynamic covalent bonds featuring good chemical resistance, stiffness, and facile processability and recyclability have attracted much attention for the fabrication of advanced materials.[4–11] Various dynamic covalent bonds, such as imine bonds, boronate ester bonds, diselenide bonds and disulfide bonds, have been reported to construct a new generation of low-cost and high-performance recyclable materials, leading to progress in materials science and polymer chemistry.[12–20]

Poly(disulfide)s (PolyTAs) made from thioctic acid (TA), a natural, renewable raw ingredient, featuring disulfide (S–S) bonds have emerged as a new class of eco-friendly polymers.[21] It has been found that PolyTAs can undergo efficient depoly-

merization and repolymerization, due to the reversible opening and closing of cyclic dynamic S–S bonds under mild stimuli—such as heat, light, or redox conditions.[22–27] In recent years, PolyTAs have made remarkable progress in the fabrication of versatile materials, such as sustainable materials with high performance, antibacterial materials, adhesives, and functional hydrogels.[28–36] To enhance the reliability and extend the service life of sustainable polymers, different strategies have been employed to enhance the mechanical properties of PolyTA-based materials. The introduction of covalent cross-linking sites improves the mechanical properties of the resulting materials, but it also weakens their recyclability.[37,38] The incorporation of reversible and dynamic supramolecular interactions can lead to enhanced mechanical performance without impairing the recyclability. Therefore, the integration of dynamic covalent bonds and reversible noncovalent interactions into polymeric networks can be a promising approach for constructing materials with compatible excellent mechanical performance and facile recyclable properties.

In view of TA's molecular structure, apart from the dynamic covalent disulfide bond, the carboxyl motif also plays important roles, as it not only serves as an active site for metal coordination but also strengthens network stability via hydrogen bonding.[21,29,32,34,39–44] The synergistic combination of dynamic covalent bonds and multiple supramolecular interactions should reinforce the mechanical performance of TA-based CANs.[33,34,36] Hence, in this work, we use noncovalent

[a] Key Laboratory of Synthetic and Natural Functional Molecule of the Ministry of Education, College of Chemistry and Materials Science, Northwest University, Xi'an 710127, Shaanxi, P. R. China. E-mail: zhengbo@nwu.edu.cn, gaolingyan@nwu.edu.cn
[b] College of Rehabilitation, Hangzhou Medical College, Hangzhou, China. E-mail: lxyjasmine2010@163.com

interactions (coordinate bonds and hydrogen bonds) and dynamic disulfide bonds synergistically to build a mechanically robust but dynamic polymer **Poly(TA-DES-Cu)**. Specifically, a low-toxicity, biodegradable deep eutectic solvent (DES) is introduced into the CAN to further fabricate a hydrogen bond network besides the hydrogen bonds between carboxyl groups.[45–47] Meanwhile, copper ions (Cu^{2+}) are also integrated to build coordination networks, which show antibacterial properties.[48] (1) The dynamic Cu^{2+}–carboxyl coordination enhances both the mechanical performance and self-healing efficiency of **Poly(TA-DES-Cu)**. (2) The hydroxyl/amine-rich functional groups in DESs exhibit dual functionalities, forming multiple hydrogen bond crosslinking sites within the polymer network to significantly enhance cohesive strength, while facilitating TA chain segment slippage to improve molecular mobility. (3) The synergistic effect of Cu^{2+} and DESs endows **Poly(TA-DES-Cu)** with enhanced and durable antibacterial properties and environmental stability. Furthermore, by coating **Poly(TA-DES-Cu)** onto nonwoven fabric surfaces, we successfully constructed multifunctional composite materials with enhanced mechanical performance and broad-spectrum antibacterial activity, providing innovative solutions for medical dressings, smart textiles, and related fields.

Results and discussion

Preparation and characterization of Poly(TA-DES-Cu)

This study employed a one-pot method to efficiently construct thioctic acid-based elastomers. DES and $CuSO_4$ were selected as two additives into the PolyTA network. In particular, the DES is made from the hydrogen bond donor urea and the hydrogen bond acceptor choline chloride through hydrogen bonding interactions. This low-melting mixture shows low toxicity, environmentally friendly behavior, thermal stability and biocompatibility. Moreover, DES can provide hydrogen bond crosslinking sites when it is introduced into the polymeric network. The increased hydrogen bond density can help to enhance the cohesive strength of the resulting polymer. Cu^{2+} is known to form metal coordination with the carboxyl groups on PolyTA. Therefore, as illustrated in Fig. 1a, different proportions of DES and $CuSO_4$ were introduced into molten thioctic acid at 120 °C, yielding a black elastomer designated as **Poly(TA-DES$_x$-Cu$_y$)** (x and y refer to the weight percentage of each component relative to TA, see the ESI† for details). This method involves two key steps: (1) thermal ring-opening polymerization of thioctic acid generating linear PolyTA chains; (2) the addition of DES and Cu^{2+} leading to the formation of a polymer network through hydrogen bonding and coordination interactions. Notably, the material demonstrates optimal performance when the additive contents of DES and $CuSO_4$ reach 10 wt% and 8 wt%, respectively (*vide infra*).

Attenuated total reflectance Fourier-transform infrared (ATR-FTIR) spectroscopy analysis (Fig. 1c) shows a blue shift of the carbonyl (C=O) stretching vibration peak from 1699 cm^{-1} (the carboxylic acid group in PolyTA) to 1703 cm^{-1} (**Poly**

(**TA-DES$_{10}$-Cu$_8$**) and **Poly(TA-Cu$_8$)**) due to Cu^{2+}–carboxyl coordination. Concurrently, the characteristic hydroxyl (–OH) vibration peak of DES at 3300 cm^{-1} disappeared completely in **Poly(TA-DES$_{10}$-Cu$_8$)** and **Poly(TA-DES$_{10}$)**, indicating that noncovalent interactions emerged between DES and PolyTA. Further evidence emerged from the blue shift of DES's C–O stretching vibrations (originally at 1110–1200 cm^{-1}) to 1140–1260 cm^{-1} in **Poly(TA-DES$_{10}$-Cu$_8$)** and **Poly(TA-DES$_{10}$)**, a phenomenon absent in **Poly(TA-Cu$_8$)**, further validating the hydrogen bond interactions between DES and PolyTA. ^{1}H NMR spectra (Fig. 1d) provided additional mechanistic insights: the carboxylic acid proton peak of PolyTA at 12.01 ppm shifts upfield to 11.71 ppm and becomes broader in **Poly(TA-DES$_{10}$-Cu$_8$)**. The choline chloride and urea proton peaks of DES all exhibit an obvious shift in **Poly(TA-DES$_{10}$-Cu$_8$)** (Fig. 1d), while the chemical shift change in **Poly(TA-DES$_{10}$)** was relatively small (Fig. S1, ESI†). These observations collectively confirm the concurrent formation of hydrogen bonding networks and metal-coordination bonds within the composite system.

The scanning electron microscopy (SEM) images of **Poly(TA-DES$_{10}$-Cu$_8$)** show a dense and non-porous surface (Fig. S2, ESI†). Energy-dispersive X-ray spectroscopy (EDS) was further employed to characterize elemental distribution, confirming the uniform distribution of characteristic elements, N and Cl (from DES) and Cu, throughout the entire layer. Differential scanning calorimetry (DSC) results demonstrate that the glass transition temperatures (T_g) of **Poly(TA-DES$_{10}$-Cu$_8$)** and **Poly(TA-Cu$_8$)** were −28.61 °C and −31.38 °C, respectively, while no discernible T_g of **Poly(TA-DES$_{10}$)** was observed (Fig. S3, ESI†). This is ascribed to the fact that the introduction of Cu^{2+} enhances network rigidity by increasing the crosslinking density of the CANs, whereas DES likely reduces the prominence of glass transition through enhanced chain segment mobility. Powder X-ray diffraction (PXRD) analysis (Fig. 1b) reveals that neither DES nor Cu^{2+} alone can suppress the crystallization of the PolyTA network. Only when both components are incorporated into the PolyTA network does the material exhibit amorphous characteristics, demonstrating that the synergistic crosslinking of dynamic coordination bonds and hydrogen bonds effectively disrupts polymer chain ordering. Thermogravimetric analysis (TGA) data show that **Poly(TA-DES$_{10}$-Cu$_8$)** exhibits good thermal stability with an initial decomposition temperature of 246 °C, significantly higher than those of **Poly(TA-DES$_{10}$)** and **Poly(TA-Cu$_8$)** (Fig. S4, ESI†).

Mechanical properties of Poly(TA-DES-Cu)

A uniaxial tensile test was further carried out to investigate the influence of DES and Cu^{2+} contents on the mechanical properties of the resulting materials. At first, the weight content of Cu^{2+} was kept constant. With increasing DES content, the fracture strain of the material improves significantly, while the tensile strength and Young's modulus exhibit a decreasing trend, and the toughness initially increases and then decreases (Fig. 2a and b). Then, the content of DES was kept constant at 10 wt% based on the above results.
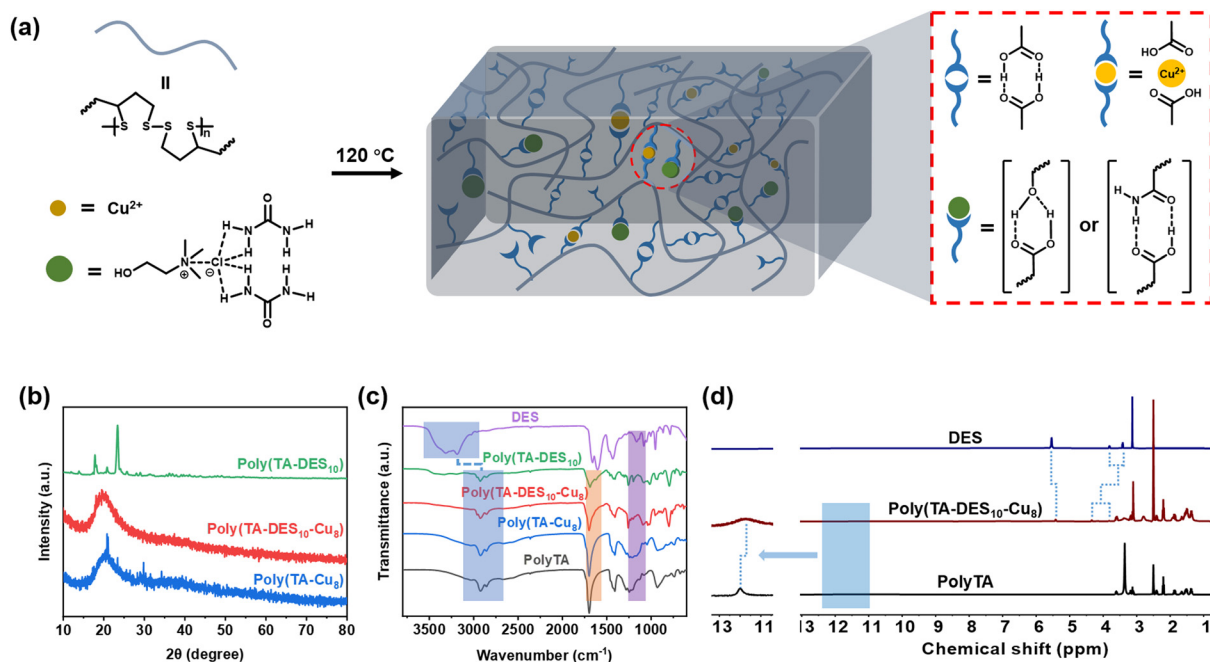
Fig. 1 (a) The schematic representation of **Poly(TA-DES-Cu)** preparation. (b) PXRD spectra of **Poly(TA-DES$_{10}$)**, **Poly(TA-DES$_{10}$-Cu$_8$)**, and **Poly(TA-Cu$_8$)**. (c) ATR-FTIR spectra of DES, **Poly(TA-DES$_{10}$)**, **Poly(TA-DES$_{10}$-Cu$_8$)**, **Poly(TA-Cu$_8$)**, and PolyTA. (d) ^{1}H NMR spectra of DES, **Poly(TA-DES$_{10}$-Cu$_8$)**, and PolyTA (400 MHz, DMSO-d_6, 298 K).
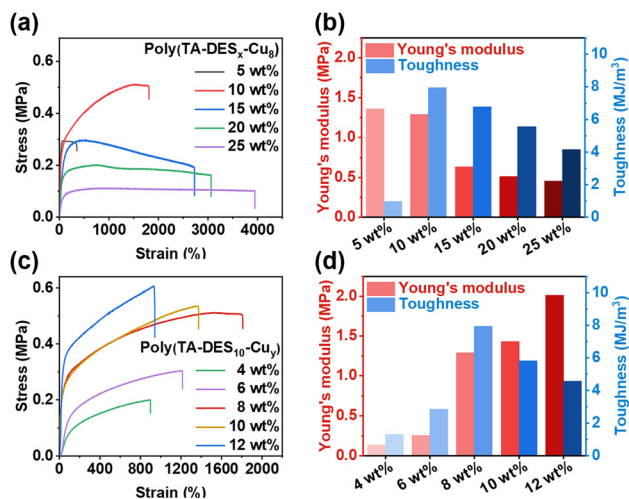

Fig. 2 (a) Tensile stress−strain curves of the resulting **Poly(TA-DES$_x$-Cu$_8$)** with different weight ratios of DES (x = 5, 10, 15, 20 and 25, respectively). (b) Young's modulus and toughness calculated from the tensile stress−strain curve of **Poly(TA-DES$_x$-Cu$_8$)**. (c) Tensile stress−strain curves of the resulting **Poly(TA-DES$_{10}$-Cu$_y$)** with different weight ratios of Cu^{2+} (y = 4, 6, 8, 10 and 12, respectively). (d) Young's modulus and toughness calculated from the tensile stress−strain curve of **Poly(TA-DES$_{10}$-Cu$_y$)**.

The incorporation of Cu^{2+} showed a distinct reinforcement effect: as the Cu^{2+} content increases, the tensile strength, fracture strain, and Young's modulus of the material all exhibit an upward trend. However, beyond a critical threshold of 8 wt%, the fracture strain and toughness begin to decline (Fig. 2c and

d). This is ascribed to the fact that Cu^{2+} leads to the formation of high-density coordination crosslinking in the polymer network, which enhances the material's stiffness, but it also restricts molecular chain slippage. Comprehensive experiments and analysis of tensile tests reveal that when the DES and Cu^{2+} contents are optimized to 10 wt% and 8 wt%, respectively, the material exhibits the best balance of mechanical properties, with a Young's modulus of 1.29 MPa, a toughness of 7.92 MJ m^{-3}, a maximum tensile strength of 0.51 MPa, and a fracture strain of 1808%. Consequently, this sample (TA : DES : CuSO$_4$ = 100 : 10 : 8, mass ratio) was selected as the representative material for further investigation.

To further validate the critical roles of DES and Cu^{2+} in enhancing the mechanical properties of **Poly(TA-DES$_{10}$-Cu$_8$)**, control PolyTA-based polymers containing solely DES (**Poly(TA-DES$_{10}$)**) or CuSO$_4$ (**Poly(TA-Cu$_8$)**) were prepared. The tensile test demonstrates that both these control polymers show much worse mechanical performance compared to that of **Poly(TA-DES$_{10}$-Cu$_8$)** (Fig. S5a, ESI†). Moreover, individual choline chloride or urea was employed as an additive into the PolyTA network. It was found that neither of these two components can inhibit the crystallization of poly(disulfide) (Fig. S5b, ESI†). These results confirm the synergistic enhancement mechanism arising from the concurrent incorporation of DES-mediated hydrogen bonding and Cu^{2+} coordination interactions in the composite system.

Through tensile/compression tests at varied strain rates, the rate-dependent mechanical behavior of **Poly(TA-DES$_{10}$-Cu$_8$)** was systematically investigated. As shown in Fig. 3a and b, increasing the deformation rate from 10 mm min^{-1} to 500 mm
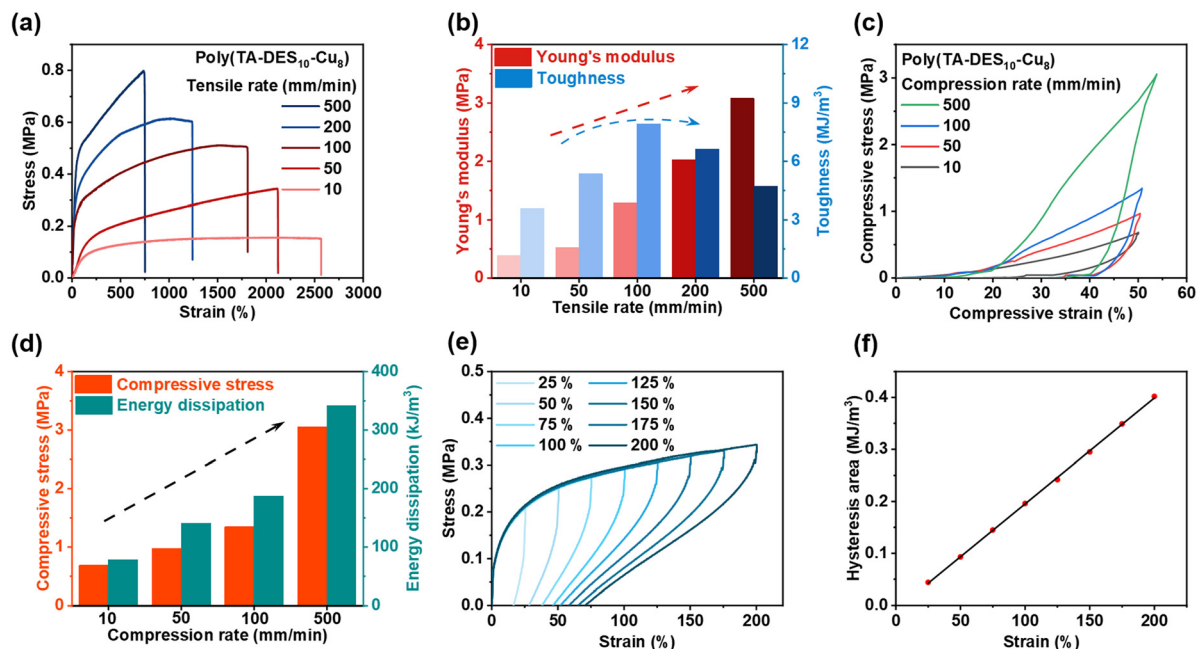
Fig. 3 (a) Tensile stress–strain curves of **Poly(TA-DES$_{10}$-Cu$_8$)** under different strain rates. (b) Young's modulus and toughness calculated from tensile stress–strain curves. (c) Compressive stress–strain curves of **Poly(TA-DES$_{10}$-Cu$_8$)** with different compression rates. (d) Compressive stress and energy dissipation of **Poly(TA-DES$_{10}$-Cu$_8$)** calculated from its cyclic compressive curves. (e) Cyclic tensile test curves of **Poly(TA-DES$_{10}$-Cu$_8$)** recorded at room temperature with increasing maximum strain. The tensile rate is 100 mm min^{-1}. (f) Hysteresis area of **Poly(TA-DES$_{10}$-Cu$_8$)** for each cycle of the tensile test.

min^{-1} leads to higher maximum tensile strength and Young's modulus, accompanied by a decrease in fracture strain. Compression tests also show this rate-dependent phenomenon. With increasing compression rates under constant strain, both compressive stress and energy dissipation demonstrate monotonic enhancement (Fig. 3c and d). Cyclic tensile tests were conducted to investigate the energy dissipation characteristics of the material. Energy dissipation was quantified by calculating the hysteresis loop area formed between the loading and unloading curves. The material exhibits significant strain accumulation within the 25–200% strain range, manifested by progressive expansion of the hysteresis loop area and gradual accumulation of residual strain with increasing cycle numbers (Fig. 3e). Furthermore, energy dissipation efficiency displays a positive correlation with the strain amplitude, with the quantitative relationship curve approximating a linear response (Fig. 3f). Under fixed 75% deformation, **Poly (TA-DES$_{10}$-Cu$_8$)** maintains a stable hysteresis loop morphology through ten consecutive loading–unloading cycles, with a peak stress decay below 8% (Fig. S6a, ESI†), confirming its excellent structural integrity and energy dissipation capability. These results are attributed to the competitive relationship between the strain rate and the characteristic relaxation time of noncovalent bonds. Under low strain rates, dynamic bonds (hydrogen bonds and coordination bonds) within the polymer network effectively dissipate energy through continuous dissociation–recombination processes; when loading rates exceed the relaxation threshold of dynamic bonds, the polymer

network loses its stress-release capability through bond reorganization and instead accumulates energy *via* elastic deformation. Remarkably, after experiencing 600% deformation, the material spontaneously recovered to its near-initial state within 30 min at ambient temperature (Fig. S6b, ESI†). This rapid self-recovery behavior originates from the reversible reconstruction of the dynamic noncovalent network.

Self-healing and reprocessability of Poly(TA-DES10-Cu8)

Poly(TA-DES$_{10}$-Cu$_8$), a dynamic crosslinked network through the synergistic integration of hydrogen bonds, metal coordination bonds, and disulfide bonds, is expected to show exceptional self-healing capability (Fig. 4).[44] As shown in Fig. 4a and b, a near-complete healing efficiency (~100%) was achieved at both 25 °C and 60 °C for the first healing cycle. Notably, after 10 consecutive damage–healing cycles at 60 °C, the material maintained over 80% stress recovery efficiency, with strain recovery comparable to its original state.

The healing process was further evaluated with different healing times (0, 10, 20, and 30 min, respectively). It was found that as the healing time increases to 30 min, the material progressively recovers to its initial state (Fig. S7, ESI†). These results reveal that the self-healing efficiency of **Poly (TA-DES$_{10}$-Cu$_8$)** is positively correlated with healing time and temperature. The possible reason for the good self-healing ability of **Poly(TA-DES$_{10}$-Cu$_8$)** should be ascribed to the highly efficient reversible bonding behavior that originates from the dynamic covalent bonds and noncovalent bonds. Specifically,
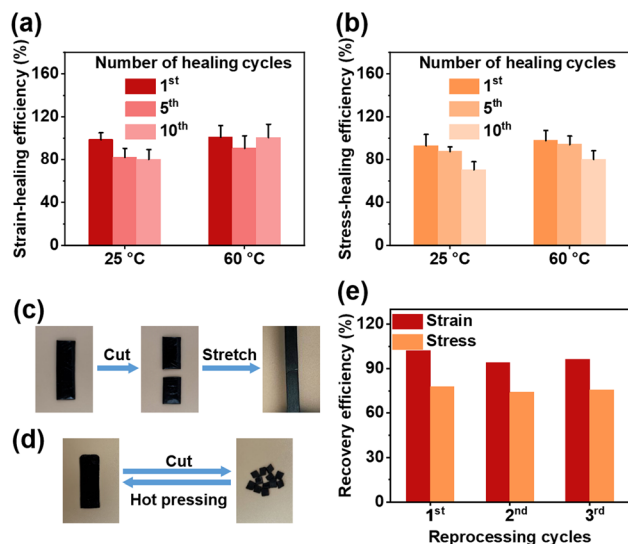
Fig. 4 Self-healing efficiency of **Poly(TA-DES$_{10}$-Cu$_8$)** at 25 and 60 °C: (a) strain, (b) stress, and (c) photographs of the self-healing of **Poly(TA-DES$_{10}$-Cu$_8$)** that was cut into two pieces. (d) Recycling of **Poly(TA-DES$_{10}$-Cu$_8$)** by hot pressing. (e) Recovery efficiency of **Poly(TA-DES$_{10}$-Cu$_8$)**.

Fig. 5 (a) Continuous cyclic adhesion tests of **Poly(TA-DES$_{10}$-Cu$_8$)** on different substrates. (b) Photographs of **Poly(TA-DES$_{10}$-Cu$_8$)** during the puncture test. (c) Puncture force–displacement curves of **Poly(TA-DES$_{10}$-Cu$_y$)** with different weight ratios of Cu^{2+} (y = 6, 8 and 10, respectively). (d) Puncture displacement, puncture force and puncture energy of **Poly(TA-DES$_{10}$-Cu$_y$)**.

the synergistic reorganization of Cu^{2+}–carboxyl coordination bonds, disulfide bonds, and hydrogen bonds in the interfacial region can form a multi-scale dynamic cross-linked network, enabling rapid healing of the interfacial surface. The increased temperature accelerates the mobility of the polymer chain, which further accelerates the reorganization of these three dynamic bonds and leads to the enhancement of the self-healing efficiency.[21,49,50]

A temperature-dependent rheological test also confirms the dynamic nature of the material and its recovery capability. During three consecutive heating–cooling cycles, the material demonstrated reversible recovery of both modulus and viscosity to their initial states (Fig. S8†). This superior healing performance arises from the multiple dynamic bonds. At elevated temperatures, both noncovalent bonds and dynamic covalent bonds at fracture interfaces are activated and establish multiple repair pathways that enhance healing efficiency.

The material also exhibits excellent reprocessability without solvents or complex procedures. Specifically, the fragmented material can be regenerated by hot-pressing at 80 °C for 20 min (Fig. 4d). Even after three reprocessing cycles, the material retains over 75% of the original stress while maintaining nearly 100% of its initial strain performance (Fig. 4e).

Adhesion and puncture properties of Poly(TA-DES10-Cu8)

Poly(TA-DES$_{10}$-Cu$_8$) also shows interfacial adhesion performance and cyclic bonding stability. Macroscopic adhesion tests revealed that the material can stably support a 10 kg load in lateral bearing tests without interfacial separation (Fig. S9†). Quantitative characterization *via* single-lap shear tests showed a bonding strength of 2.52 MPa on steel substrates, with a
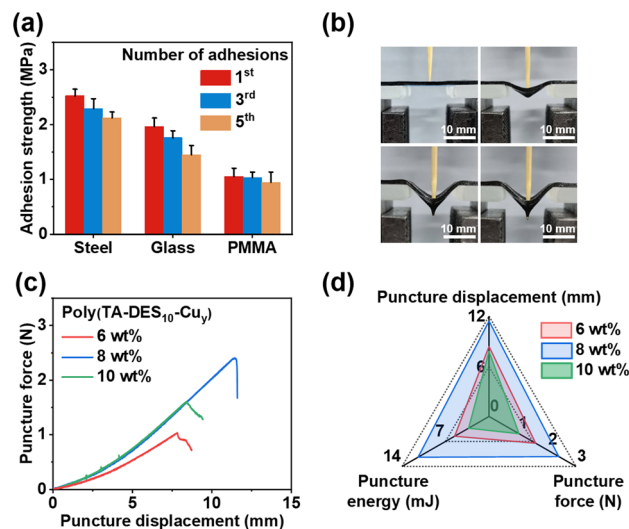
retained strength of 2.12 MPa after five bonding–debonding cycles (Fig. 5a). During the adhesion process, the abundant carboxyl groups on the poly(disulfide) network endow the material with excellent interfacial adhesive properties on the substrate surfaces.[6] Moreover, the hydroxyl/amine-rich functional groups in DES further provide noncovalent interactions between the polymeric surface and the substrate. As stronger metal–carboxyl coordination is formed between the polymer and the steel surface, the polymer shows the best adhesive ability to steel. In addition, after interface separation, initial bonding performance was restored through a 5 min thermal treatment at 60 °C, enabling rapid interfacial reconstruction. This cycling stability originates from the material's intrinsic self-healing properties as thermally activated dynamic bond reorganization facilitates rapid reconstruction of noncovalent networks at fractured interfaces.

Poly(TA-DES$_{10}$-Cu$_8$) exhibits excellent anti-puncture properties. Puncture experiments were performed using a 400 μm toothpick tip as the puncture tool (Fig. 5b). A maximum puncture displacement of 11.41 mm, a puncture energy dissipation of 11.42 mJ, and a peak puncture force of 2.41 N were achieved for **Poly(TA-DES$_{10}$-Cu$_8$)** (Fig. 5c and d). This performance is speculated to arise from the dissociation–reorganization of Cu^{2+}–carboxyl coordination bonds under external stress that effectively alleviates stress concentration at the puncture tip and chain slippage mediated by DES that continuously dissipates mechanical energy through viscoelastic deformation. The synergistic interaction between dynamic bond networks and molecular chain mobility enables significant enhancement of structural damage resistance while maintaining material flexibility.
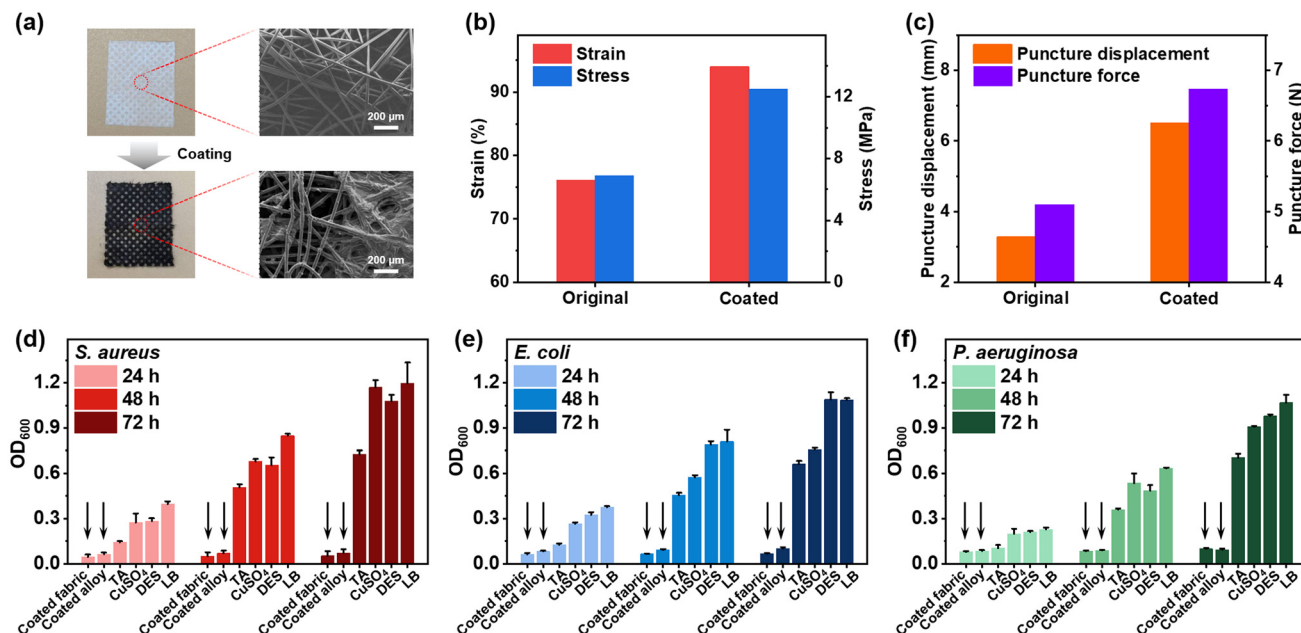
Fig. 6 (a) SEM images of original and coated non-woven fabrics. (b) Strain and stress curves of original and coated non-woven fabrics. (c) Puncture force and displacement of original and non-coated woven fabrics. Antibacterial ability of the titanium alloy and non-woven fabric coated with **Poly (TA-DES$_{10}$-Cu$_8$)**, TA, CuSO$_4$ and DES, respectively, against (d) *S. aureus*, (e) *E. coli*, and (f) *P. aeruginosa*.

Coating application

Novel coating materials that integrate environmental friendliness and multiple functions have garnered increasing attention. Based on the natural biomolecule TA and green DES as raw materials, **Poly(TA-DES-Cu)** is a kind of sustainable material and shows various advanced properties. We further applied this material to construct coatings with multiple functions. The **Poly(TA-DES-Cu)** coating can be easily prepared on the surfaces of titanium alloys (Fig. S10†) or nonwoven fabrics (Fig. 6a). Taking nonwoven fabric as an example, SEM images show that the **Poly(TA-DES$_{10}$-Cu$_8$)** coating forms a continuous coating surface on the nonwoven fabric *via* a dip-coating process (Fig. 6a). EDS analysis confirms the uniform distribution of N, Cl, and Cu elements across the fiber surface (Fig. S11†), verifying homogeneous coating deposition. Notably, the **Poly(TA-DES$_{10}$-Cu$_8$)**-coated nonwoven fabric exhibited significant mechanical enhancement in tensile strength, fracture strain and puncture resistance (Fig. 6b, c and S12†). The tensile strength of the **Poly(TA-DES$_{10}$-Cu$_8$)**-coated nonwoven fabric enhances from 6.87 MPa to 12.51 MPa (+182%), while the Young's modulus increases from 19.13 MPa to 66.36 MPa (+347%).

The **Poly(TA-DES$_{10}$-Cu$_8$)** coating can further improve the ductility of nonwoven fabrics, increasing the fracture strain from 76% to 93% (+122.4%). More importantly, the coating endows the nonwoven fabric with puncture resistance. The **Poly(TA-DES$_{10}$-Cu$_8$)**-coated nonwoven fabric shows a maximum displacement of 6.51 mm (+198.5%), a peak puncture force of 6.73 N (+131.7%), and a puncture energy dissipation capacity of 13.33 mJ (+127.5%). These improvements in the mechanical

performance of the **Poly(TA-DES$_{10}$-Cu$_8$)**-coated nonwoven fabric stem from the energy dissipation mechanism of the dynamic noncovalent bonds of the **Poly(TA-DES$_{10}$-Cu$_8$)** coating under external forces that effectively disperse stress concentration while maintaining the substrate's inherent flexibility.

Previous studies have confirmed the inherent antibacterial properties of PolyTA.[34] As a result, we further investigated the antimicrobial efficacy of **Poly(TA-DES$_{10}$-Cu$_8$)** coatings on titanium alloy and nonwoven fabric substrates. To systematically evaluate antibacterial performance, substrates coated with **Poly (TA-DES$_{10}$-Cu$_8$)** were co-cultured with *S. aureus*, *E. coli* and *P. aeruginosa* in LB broth, with control groups containing pure TA, CuSO$_4$, DES, and blank LB solution. The results demonstrated that even after 3 days of co-culturing, the **Poly (TA-DES$_{10}$-Cu$_8$)**-coated substrates exhibit over 96% antibacterial efficiency against all three bacterial strains (Fig. 6d–f). These findings not only confirm the significant antimicrobial enhancement imparted by the **Poly(TA-DES$_{10}$-Cu$_8$)** coating but also reveal its exceptional broad-spectrum antibacterial activity across diverse bacterial species. Moreover, the enhanced tensile strength and puncture resistance of the non-woven fabric coated with **Poly(TA-DES$_{10}$-Cu$_8$)** may provide a new strategy for developing high-performance coatings in the area of technical textile materials.

Conclusion

This study successfully constructed a mechanically robust but dynamic elastomer through the synergistic integration of

dynamic disulfide bonds and noncovalent interactions. The dynamic Cu^{2+}–carboxyl coordination reinforces the mechanical performance and self-healing efficiency of the elastomer, while the increased hydrogen bond crosslinking sites brought about by DES remarkably improve the polymer's cohesive strength and molecular mobility. More importantly, it can be easily applied to construct environmentally friendly coating surfaces on titanium alloys and nonwoven fabrics, simultaneously improving substrate mechanical performance and imparting enhanced and durable broad-spectrum antibacterial activity. Through rational design of reversible noncovalent networks, this material system achieves integration of mechanical properties, environmental compatibility, and multifunctionality, providing a novel strategy for developing next-generation intelligent polymer materials.

Conflicts of interest

There are no conflicts to declare.

Data availability

The data supporting this article have been included as part of the ESI.†

Acknowledgements

References

1 M. Rottger, T. Domenech, R. Weegen, A. Breuillac, R. Nicolay and L. Leibler, *Science*, 2017, **356**, 62–65.
2 Y. Jin, Z. Lei, P. Taynton, S. Huang and W. Zhang, *Matter*, 2019, **1**, 1456–1493.
3 S. Park, H. Jeon, H. Kim, S. Shin, S. Choy, D. Hwang, J. Koo, J. Jegal, S. Hwang, J. Park and D. Oh, *Nat. Commun.*, 2019, **10**, 2601.
4 G. Li, L. Wang, L. Wu, Z. Guo, J. Zhao, Y. Liu, R. Bai and X. Yan, *J. Am. Chem. Soc.*, 2020, **142**, 14343–14349.
5 Y. Zhang, L. Zhang, G. Yang, Y. Yao, X. Wei, T. Pan, J. Wu, M. Tian and P. Yin, *J. Mater. Sci. Technol.*, 2021, **92**, 75–87.
6 Q. Zhang, D.-H. Qu, B. Feringa and H. Tian, *J. Am. Chem. Soc.*, 2022, **144**, 2022–2033.
7 Z. Hu, F. Hu, L. Deng, Y. Yang, Q. Xie, Z. Gao, C. Pan, Y. Jin, J. Tang, G. Yu and W. Zhang, *Angew. Chem., Int. Ed.*, 2023, **62**, e202306039.
8 Y. Shen, Q. Jia, S. Xu, J. Yu, C. Huang, C. Wang, C. Lu, Q. Yong, J. Wang and F. Chu, *Adv. Funct. Mater.*, 2023, **34**, 2310599.
9 L. Chen, W. You, J. Wang, X. Yang, D. Xiao, H. Zhu, Y. Zhang, G. Li, W. Yu, J. Sessler and F. Huang, *J. Am. Chem. Soc.*, 2024, **146**, 1109–1121.
10 Z. Lei, H. Chen, S. Huang, L. Wayment, Q. Xu and W. Zhang, *Chem. Rev.*, 2024, **124**, 7829–7906.
11 J. Zhao, Z. Zhang, C. Wang and X. Yan, *CCS Chem.*, 2024, **6**, 41–56.
12 S. Wang, X. Xing, X. Zhang, X. Wang and X. Jing, *J. Mater. Chem. A*, 2018, **6**, 10868–10878.
13 N. Zheng, Y. Xu, Q. Zhao and T. Xie, *Chem. Rev.*, 2021, **121**, 1716–1745.
14 X. Zhang, J. Zhao, K. Liu, G. Li, D. Zhao, Z. Zhang, J. Wan, X. Yang, R. Bai, Y. Wang, W. Zhang and X. Yan, *Natl. Sci. Rev.*, 2022, **9**, nwac012.
15 K. Chen, C. Cui, Z. Li, Z. Song, Q. Zhang, Y. Wu, Z. Ge, Y. Cheng and Y. Zhang, *ACS Macro Lett.*, 2023, **12**, 543–548.
16 X. Xiao, D. Xiao, G. Sheng, T. Shan, J. Wang, X. Miao, Y. Liu, G. Li, Y. Zhu, J. Sessler and F. Huang, *Sci. Adv.*, 2023, **9**, eadi1169.
17 P. Yu, H. Wang, Y. Wang, D. Liu, Y. Xin, R. Li, X. Jia, L. Liu, D. Zhang, C. Wang, J. Zhao, Z. Zhang and X. Yan, *Chem. – Eur. J.*, 2023, **29**, e202203560.
18 S.-W. Zhou, C. Yu, M. Chen, C.-Y. Shi, R. Gu and D.-H. Qu, *Smart Mol.*, 2023, **1**, e20220009.
19 H. Wang, Q. Huang, C. Liu, W. Hong, J. Li, J. Ma, P. Yu, C. Wang and X. Yan, *Chem. – Eur. J.*, 2024, **30**, e202401481.
20 R. Bai, W. Wang, W. Gao, Z. Zhang, W. Yu and X. Yan, *Angew. Chem., Int. Ed.*, 2025, e202423578.
21 Q. Zhang, C.-Y. Shi, D.-H. Qu, Y.-T. Long, B. Feringa and H. Tian, *Sci. Adv.*, 2018, **4**, eaat8192.
22 C. Cai, S. Wu, Z. Tan, F. Li and S. Dong, *ACS Appl. Mater. Interfaces*, 2021, **13**, 53083–53090.
23 C.-Y. Shi, Q. Zhang, B.-S. Wang, M. Chen and D.-H. Qu, *ACS Appl. Mater. Interfaces*, 2021, **13**, 44860–44867.
24 C. Cai, S. Wu, Y. Zhang, F. Li, Z. Tan and S. Dong, *Adv. Sci.*, 2022, **9**, e2203630.
25 X. Lan, L. Boetje, T. Pelras, C. Ye, F. Silvianti and K. Loos, *Polym. Chem.*, 2023, **14**, 5014–5020.
26 C. Cui, F. Wang, X. Chen, T. Xu, Z. Li, K. Chen, Y. Guo, Y. Cheng, Z. Ge and Y. Zhang, *Adv. Funct. Mater.*, 2024, **34**, 2315469.
27 Y. Deng, Z. Huang, B. Feringa, H. Tian, Q. Zhang and D.-H. Qu, *Nat. Commun.*, 2024, **15**, 3855.
28 J. Li, S. Luo, F. Li and S. Dong, *ACS Appl. Mater. Interfaces*, 2022, **14**, 27476–27483.
29 J. Li, Y. Zhang, Q. Zhang, C. Cai, F. Li and S. Dong, *Adv. Mater. Interfaces*, 2022, **10**, 2202005.
30 J. Du, F. Wang, J. Li, Y. Yang, D. Guo, Y. Zhang, A. Yang, X. He and Y. Cheng, *Biomater. Sci.*, 2023, **11**, 3683–3694.
31 Y. Zhang, C. Cai, F. Li and S. Dong, *Small*, 2023, **19**, e2300857.
32 H. Qiao, B. Wu, S. Sun and P. Wu, *J. Am. Chem. Soc.*, 2024, **146**, 7533–7542.

33 D. Yang, K. Zhao, R. Yang, S.-W. Zhou, M. Chen, H. Tian and D.-H. Qu, *Adv. Mater.*, 2024, **36**, e2403880.

34 Y. Zhang, C. Cai, K. Xu, X. Yang, L. Yu, L. Gao and S. Dong, *Mater. Horiz.*, 2024, **11**, 1315–1324.

35 G. Yao, M. Gao, Q. Zhang, X. Tan, C. Cai and S. Dong, *Adv. Mater. Interfaces*, 2025, 2500648.

36 Y. Zhang, C. Cai, Z. Guo, X. Li, G. Zhao and S. Dong, *Mater. Horiz.*, 2025, **12**, 2287–2297.

37 M. Chen, R. Yang, H. Wu, Q. Wang, C. Shi, S.-W. Zhou, D. Yang, F.-Y. Liu, H. Tian and D.-H. Qu, *Angew. Chem., Int. Ed.*, 2024, **63**, e202409200.

38 M. Shi, C. Shi, Q. Zhang and D.-H. Qu, *Chem. Eng. J.*, 2024, **484**, 149564.

39 R. Castañeda, J. Alvarez and N. Mora, *RSC Adv.*, 2016, **6**, 107924–107932.

40 C. Cui, B. Liu, T. Wu, Y. Liu, C. Fan, Z. Xu, Y. Yao and W. Liu, *J. Mater. Chem. A*, 2022, **10**, 1257–1269.

41 J. Li, Y. Zhang, Q. Zhang, C. Cai, F. Li and S. Dong, *Adv. Mater. Interfaces*, 2022, **10**, 2202005.

42 S.-W. Zhou, F. Tong, M. Chen, R. Gu, C.-Y. Shi, C.-Y. Yu, Q. Zhang and D.-H. Qu, *Angew. Chem., Int. Ed.*, 2022, **61**, e202117195.

43 C.-Y. Shi, D.-D. He, B.-S. Wang, Q. Zhang, H. Tian and D.-H. Qu, *Angew. Chem., Int. Ed.*, 2023, **62**, e202214422.

44 Y. Zhang, C. Cai, F. Li and S. Dong, *Small*, 2023, **19**, e2300857.

45 J. Li, M. Zhang, J. He and P. Ni, *Chem. Commun.*, 2023, **59**, 8814–8817.

46 X. Jiang, Y. Hou, Y. Wang, F. Chu, J. Zhu, L. Song, Y. Hu and W. Hu, *Adv. Funct. Mater.*, 2024, **35**, 2412313.

47 W. Xu, T. Shen, Y. Ding, H. Ye, B. Wu and F. Chen, *Small*, 2024, **20**, e2310072.

48 T. Yang, H. Xu, Z. Liu, Y. Xiao, X. Fu, Y. Lei, J. Lei and L. Jiang, *Adv. Funct. Mater.*, 2024, 2419308.

49 J. Xu, T. Liu, Y. Zhang, Y. Zhang, K. Wu, C. Lei, Q. Fu and J. Fu, *Matter*, 2021, **4**, 2474–2489.

50 F. Sun, J. Zhang, T. Liu, H. Yao, L. Wang, H. Meng, Y. Gao, Y. Cao, B. Yao, J. Xu and J. Fu, *Adv. Mater.*, 2024, **36**, e2410650.